PHASE STUDIES IN III–IV, II–VI, AND IV–VI COMPOUND SEMICONDUCTOR ALLOY SYSTEMS

M. Ilegems
Bell Laboratories, 600 Mountain Avenue, Murray Hill, New Jersey 07974

G. L. Pearson
Department of Electrical Engineering, Stanford University, Stanford, California 94305

INTRODUCTION

A large number of systems based on III–V, II–VI, and IV–VI compounds exhibit complete solid miscibility or extensive composition ranges over which solid solutions can be formed. In these systems, the solid phase is a phase of variable composition with respect to two or more of the components; the composition variation allows one to obtain intermediate combinations of properties as compared with the properties of the initial compounds. The compound alloys find extensive applications in semiconductor devices that require a certain well-defined energy band structure, such as light or electron emitters, detectors, and heterojunction injection lasers. At present, most attention is centered on the III–V and IV–VI alloy systems that can be amphoterically doped and in which bandgaps extending from the far infrared to the visible green can be realized. In addition to these systems whose technology is presently well developed, a strong interest also exists in the II–VI compound solutions as well as in the (II–VI)–(III–V) and (II–VI)–(IV–VI) mixtures, mainly in view of the potential such alloys may hold for extending the bandgap region over which these II–VI compound-based systems can be amphoterically doped.

The major difficulty in the growth of homogeneous alloy crystals from dilute or stoichiometric melts results from the differences in the equilibrium compositions of the liquid and solid phases, which leads to segregation during solidification and compositional variations in the grown crystals. A knowledge of the phase relationships that govern the growth of such alloys from solution is therefore essential.

This paper discusses recent work concerning both the thermodynamic properties of solid solution alloys and the liquid-solid phase equilibrium conditions for growth of these alloys from ternary or quaternary solutions. No attempt is made to

provide a complete survey of the literature on the subject. Rather, characteristic examples of specific III–V, II–VI, and cubic IV–VI systems are treated in some detail to illustrate the significant aspects and common features of the phase diagrams and to underline their implications with regard to alloy crystal growth.

For a more detailed discussion of some of the topics covered here we refer to several recent reviews. Panish & Ilegems (1) treated the thermodynamic aspects of III–V solution growth and summarized the available experimental information on ternary III–V phase diagrams. Stringfellow (2), Foster (3), and Kressel & Nelson (4) reviewed the thermodynamic properties and phase studies in III–V systems with emphasis in the two latter papers on crystal growth and device aspects. Mullin & Hurle (5) analyzed the gas phase equilibria during vapor deposition of III–V mixed crystals. In the field of II–VI and IV–VI compound alloys much of the available thermochemical information up to 1967 has been summarized in the monograph by Abrikosov et al (6). Some of the more recent work on IV–VI mixed crystals in relation to narrow gap semiconductor applications is discussed by Harman & Melngailis (7).

THERMODYNAMICS OF SOLID SOLUTIONS

Relation Between Thermodynamic and Electronic Properties of Binary Compounds

The group III–V and II–VI compounds crystallize in the sphalerite (cubic) or wurtzite (hexagonal) structures. The bonding is tetragonal and predominantly covalent in nature as a consequence of the sp^3 hybridization of the valence band ground state. The IV–VI compounds crystallize in either the NaCl (cubic) or orthorhombic structure. The bonding has sixfold symmetry and is predominantly covalent, with the valence band ground state made up of p^3 orbitals. Extensive solid solution ranges are observed between compounds with differing crystal structures (e.g. cubic ZnSe and hexagonal ZnS), which indicates that the nature of the bonding is similar in the two crystal modifications.

The nature of the bonding and the physical properties of the compounds, as expressed by their electronic band structure, are intimately related. Using a simplified one-gap band structure representation, Phillips and Van Vechten (8–10) developed a unified model for the semiconductor solid that relates physical and chemical characteristics such as crystal structure, ionicity, heats of formation, and heats of fusion to the electronic properties. The model is based on the concept of an average energy gap E_g that represents a weighted average of all valence-to-conduction bandgaps in the crystal and whose value is obtained from the experimental static dielectric constant ε_0. In sequences of compounds having approximately the same lattice constant (e.g. Ge, GaAs, ZnSe), the bandgap increases with increasing electronegativity difference between the constituent elements of the compound. Within a group of compounds made up of elements from the same columns in the periodic table the bandgap increases with decreasing lattice constant. To represent these features the average energy gap E_g is separated into homopolar (E_h) and ionic (C) components according to

$$E_g^2 = E_h^2 + C^2 \qquad 1.$$

C is defined as the electronegativity difference for the bond and is proportional to the coulombic potential difference between ion cores screened by the valence electrons. To account for the lattice constant dependence, the homopolar energy gap E_h is assumed to be a function of nearest neighbor distance r only. The dependence of E_h on r is expressed (8) by a power law formula

$$E_h(r) = E_{h,\mathrm{Si}} \times (r/r_{\mathrm{Si}})^{-2.5} \qquad 2.$$

where the constant coefficient and the exponent are chosen to fit the values of E_h (determined from the experimental dielectric constant) for Si and diamond. From the average heteropolar and homopolar energy gaps the fractional ionicity of the bond is defined as

$$f_i = C^2/(E_h^2 + C^2) \qquad 3.$$

For covalent crystals with formula AB it is found that tetragonal bonding occurs when $f_i \leqq 0.785$, while for larger values of f_i the bonding is octahedral.

From the knowledge of the parameters that describe the covalent and ionic parts of the bonding, the thermodynamic properties of the compounds can be estimated. By evaluating the different contributions to the bonding energy, the heat of formation for these compounds can be expressed as (11)

$$-\Delta H^f_{\mathrm{AB}} = \Delta H_0 f_{i,\mathrm{AB}} D_{\mathrm{AB}} (a_{\mathrm{AB}}/a_0)^{-3} \qquad 4.$$

In this expression $(a_{\mathrm{AB}}/a_0)^{-3}$ represents the covalent contribution to the bonding, assumed to be a power law function of lattice constant only with the exponent determined empirically to give a good fit for compounds containing first row atoms; f_i represents the ionic contribution to the bonding; D is a dehybridization factor accounting for the reduction of the sp^3 covalent bond strength resulting from the presence of d-level electrons; and $\Delta H_0\, a_0^3$ is a constant scaling factor chosen by fitting the available experimental data. Agreement between the experimental heats of formation for III–V and II–VI compounds and the values calculated using Equation 4 is often within 1–2 kcal/mol and may be considered very good in view of the fact that only one constant scaling factor is involved in fitting the experimental results. Representative values for a number of compounds are listed in Table 1.

The cohesive energy (or energy of atomization) of the crystal constitutes a more fundamental bulk property than the heat of formation, as this energy is measured relative to the energies of the isolated components of the crystal and thus is independent of the particular aggregate state and phase of these components at some reference temperature and pressure. For the cohesive energies, a simple functional dependence on ionicity is also observed in sequences of crystals having approximately equal bond lengths (e.g. Ge, GaAs, ZnSe). These cohesive energies are found to be nearly linear in f_i and can be represented by the relation (10)

$$\Delta G^{at}(R, f_i) = \Delta G^{at}(R, 0)[1 - k(R) f_i] \qquad 5.$$

where R is the average row number of the compound and $k(R)$ a proportionality factor.

Van Vechten (12) has evaluated the heats and entropies of fusion in terms of the

Table 1 Calculated and experimental formation enthalpies for selected compounds[a]

Crystal	ΔH^f (calc) kcal/mol	ΔH^f (exp) kcal/mol
GaP	26.9	24.4
GaAs	17.0	17
GaSb	9.2	10
InP	20.4	21.2
InAs	11.3	14.0
InSb	8.2	7.3
ZnS	45.9	49.2
ZnSe	41.4	39
ZnTe	25.1	28.1
CdS	36.2	38.7
CdSe	30.0	
CdTe	22.9	22.1

[a] After Phillips & Van Vechten (11).

dielectric model for the tetrahedral semiconductors that are metallic in their liquid state by considering the energy change in the transitions: solid semiconductor → solid metal → liquid metal. The following expression for ΔH^F results

$$\Delta H^F = \Delta E + \Delta E_m^F + p\Delta V^F \qquad 6.$$

where ΔE represents the difference in internal energy between the semiconductor solid and a (hypothetical) solid metal of the same material, ΔE_m^F represents the difference in internal energy between solid and liquid metal phases scaled to the experimental ΔH^F of Si, and $p\Delta V^F$ is the pressure-times-volume change upon melting. Similarly, the entropy of fusion is divided into four terms:

$$\Delta S^F = S_m^F + S_b^F + R\ln 4 + \partial(\Delta E)/\partial T|_V \qquad 7.$$

where ΔS_m^F and ΔS_b^F denote, respectively, the entropy of fusion of the solid metallic phase of the same material and the entropy of dissociation that occurs when the semiconductor transforms to a metallic liquid. $R\ln 4$ represents the entropy of mixing of the liquid phase (assumed ideal) and $\partial(\Delta E)/\partial T$ represents the entropy increase between 0°K and the melting point. The first two terms in Equation 7, $\Delta S_m^F + \Delta S_b^F$, are independent of composition and their sum is fixed empirically at 15.66 cal/mol°K in order to match the experimental ΔS^F value in Si.

Table 2 lists experimental values for the heats, entropies, and temperatures of fusion for a number of III–V and II–VI compounds for which these values are available, together with values calculated using Equations 6 and 7. For comparison, entropies of fusion estimated by summation of the experimental values observed in the group IV elements are also shown. In general, we find for the III–V compounds reasonable agreement with regard to the heats of fusion but fairly poor agreement with regard to the entropies of fusion, based on Equation 7.

As a result, calculated temperatures of fusion ($T^F = \Delta H^F/\Delta S^F$) may sometimes differ from the actual values by more than 200°C. In the case of the II–VI and IV–VI compounds, the calculations considerably overestimate the experimental determinations, probably as a result of the large degree of association in the II–VI and IV–VI liquids near the melting point.

Extension to Substitutional Alloys

Since the dielectric band model closely represents the chemical trends in the bandgaps and formation energies of the pure compounds, one would expect that the model would also be able to interpolate these trends between pure compounds in the substitutional alloys. The application of the model to the electronic structure of the alloys was investigated by Van Vechten & Bergstresser (16), who calculated the dependence on composition of the various critical point features of the optical spectrum. Similarly, the formula given earlier (Equation 4) for the heat of formation of a binary compound can be applied directly to the substitutional alloys, assuming that both the lattice constant a and the ionicity f_i vary linearly with composition, and taking into account the compositional dependence of the various critical point features that enter in the calculation of the dehybridization factor D. The heat of mixing ΔH^m of a substitutional alloy $A_xB_{1-x}C$

$$\Delta H^m = \Delta H^f_{A_xB_{1-x}C} - x\Delta H^f_{AC} - (1-x)\Delta H^f_{BC} \qquad 8.$$

where the quantities ΔH^m and ΔH^f are evaluated at the same temperature, can then be calculated as a function of composition. The results of Van Vechten (17) show a calculated variation of ΔH^m with composition that is approximately parabolic and symmetrical around the midcomposition point for most systems. The dominant terms determining the magnitude of ΔH^m, calculated using Equation 8, result from

Table 2 Experimental and calculated values for heats and entropies of fusion for several III–V and II–VI compounds[a]

	ΔH^F (exp) kcal/mol	ΔS^F (exp) cal/mol°K	T^F (exp) °C	ΔH^F (calc) kcal/mol	ΔS^F (calc) cal/mol°K	T^F (calc) °C	ΔS^F (est) cal/mol°K
AlSb	19.6	14.74	1065	22.2	16.5	1071	15.2
GaAs	25.2	16.64	1238	21.8	16.3	1067	17.4
GaSb	15.6	15.80	710	15.9	16.2	710	15.3
InAs	17.6	14.52	942	15.7	15.8	720	15.3
InSb	11.4	14.32	525	11.6	15.6	472	13.2
ZnTe	15.6	10.0	1290	27.0	16.3	1384	—
CdSe	10.5	6.9	1252	29.5	16.1	1562	—
CdTe	12.0	8.8	1092	26.3	16.1	1358	—

[a] Experimental heats and entropies of fusion after Lichter & Sommelet (13) and Kulwicki (14). ΔS^F (est) (last column) from Panish & Ilegems (1) obtained by averaging fusion entropies of corresponding group IV elements following a method suggested by Thurmond (15). Calculated ΔH^F, ΔS^F, T^F after Van Vechten (12).

the dependence of ΔH^f on lattice constant and from the sublinear variation of the dehydridization factor D with composition.

From the calculated heats of mixing, solid solution interaction parameters in a strictly regular solution approximation

$$\Delta H_m = \alpha^s x(1-x) \qquad 9.$$

may be obtained. Stringfellow (18) has shown that for many systems the calculated parameters and those obtained by curve fitting the experimental phase data are reasonably similar, taking into account the uncertainty in the fitting procedure. For other systems, however, such as GaP–InP, AlAs–GaAs, and AlAs–InAs, the results

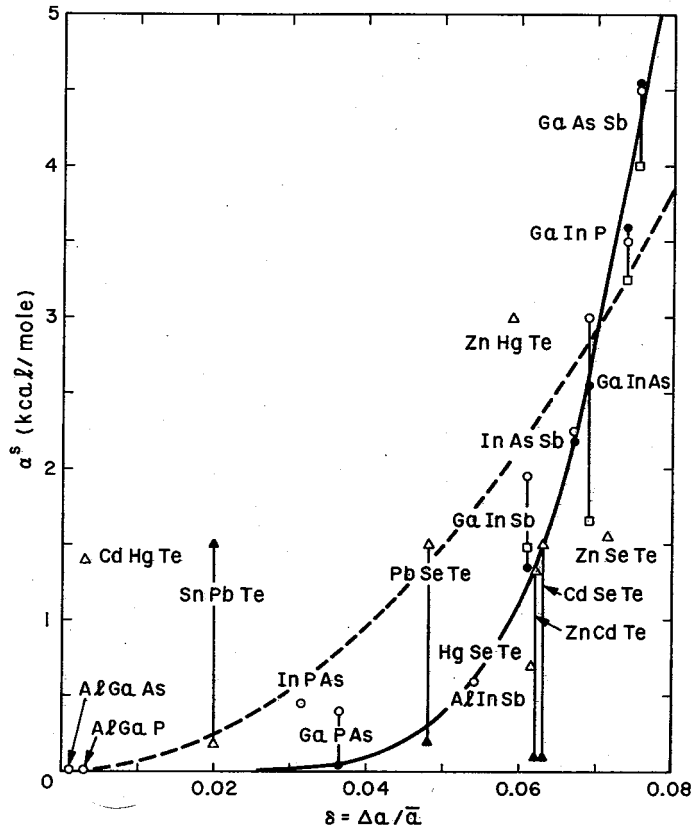

Figure 1 Solid solution interaction parameter for III–V, II–VI, and IV–VI substitutional solid solutions of type AC-BC or AB-AC. Experimental points obtained by fitting quasibinary phase data: ○ Panish & Ilegems (1), □ Foster (22), ● Brebrick & Panlener (21), △ Laugier (23), ▲ this work (Figures 12, 13). Best-fit lines to the results for III–V alloys according to Brebrick & Panlener (21), solid, and Stringfellow (19), dashed line.

appear to be definitely incorrect. Large errors are expected from the fact that the heats of mixing in systems showing complete miscibility are quite small (≤ 1 kcal/mol) compared to the uncertainty associated with the theoretical estimates for the heats of formation entering into Equation 8.

Heats of mixing can also be estimated, in a manner formally identical to Equation 8, on the basis of the difference between the cohesive energy of the alloy and that of its constituent compounds. By neglecting the dependence of the cohesive energies on ionicity and by assuming that these energies scale with the lattice constant according to an a^{-3} law in the same manner as the heats of formation, Equations 8 and 9, evaluated at $x = 0.5$, yield

$$\alpha^s = k(a_0/\bar{a})^3\delta^2 \qquad 10.$$

where $\bar{a} = (a_1 + a_2)/2$ represents the average of the lattice constants of the end components and $\delta = |a_1 - a_2|/\bar{a}$ measures the lattice parameter mismatch. The fit of Equation 10 to the available experimental data in the III–V systems has been examined by Stringfellow (19). A simple proportionality between α^s and δ^2 has also been noted previously by Urusov (20) for the heats of mixing of ionic solid solutions such as the alkali halides and chalcogenides. In one other recent analysis of pseudobinary data by Brebrick & Panlener (21), a sixth power dependence of α^s with δ as well as a linear temperature dependence for α^s were suggested.

At present there appears to be insufficient data to extract uniquely defined values for the solid interaction parameters and hence to distinguish between the square and sixth power laws on this basis. This point is illustrated in Figure 1 where values of α^s fitted to experimental data by several authors are compared with the proposed power law expressions (19, 21). In addition, it should be noted that all values of α^s obtained by fitting pseudobinary solidus data depend on the model used to represent the liquid phase and are again, therefore, not uniquely defined. This latter point was demonstrated convincingly by Steininger (24), who showed, for several pseudobinary systems, that given either the liquidus line or the solidus line, the other boundary can be calculated quite accurately assuming ideal solution behavior.

Foster & Woods (25, 26) calculated solidus and liquidus interaction parameters for several III–V alloys as a function of composition along the pseudobinary. The values of α^l/RT and α^s/RT obtained were either constant or varied slightly and about linearly with composition. The composition dependence, however, is very weak and may probably be neglected, at least in the range of these pseudobinary investigations. This is especially so because the calculation of α^s and α^l from the width of the pseudobinary gap becomes increasingly sensitive to experimental errors as one moves away from the midcomposition range because of the presence of terms in x^2 or $(1-x)^2$ in the denominators.

The question regarding the temperature dependence of α^s is still not fully resolved. A direct method for measuring activities in the solid solution is not available, so that the validity of any solution model for the solid can only be verified by comparing experimental and calculated phase diagrams. This latter method is rather insensitive. When only pseudobinary results are available, the temperature

range of the data is often insufficient to establish a temperature trend for α^s. A wider temperature range is covered when solidus data on crystals grown from metal-rich solutions are included. In this latter case, taking the Ga-In-As and Ga-In-P systems as examples, fits by Wu & Pearson (27) and McVittie (28) to the solidus data were carried out assuming an interaction parameter α^s that decreases linearly with decreasing temperature. However, the best-fit parameters to ternary phase data are not always unique when such data cover only rather limited regions of the phase diagram. Further experimental data may therefore be needed before the enthalpy and entropy contributions to the excess free energies of mixing can be evaluated separately.

REPRESENTATIONS OF LIQUID SOLUTIONS IN THE III–V, II–VI, AND IV–VI SYSTEMS

III–V Liquids

The T-x phase diagrams of the III–V systems are dominated by the presence of a near-stoichiometric, congruently melting solid phase with high melting point. In general, the eutectic on the metal side is degenerate, so that the liquidus line rises monotonically from the melting point of the metal to the melting point of the solid compound. At the melting point, the liquidus curve is parabolic with a large radius of curvature, suggesting that no appreciable association in the form of III–V complexes occurs in the liquid.

Experimental determinations of the binary p-T-x phase diagrams have been reported for most sphalerite III–V compounds with the exception of Al-P and Al-As, for which only the melting points are known, and of the Al-Sb system where vapor pressures have not yet been measured. References to the experimental liquidus determinations have been summarized in (1). Typical liquidus diagrams, taking the Ga-As and In-P systems as examples, are shown in Figure 2.

Several models have been used for the analytical representation of the III–V solutions from analyses of the liquidus data. These include, listed roughly in order of increasing strictly s-regular complexity, the solution model [Vieland (30)], the simple solution model [Thurmond (15), Panish & Ilegems (1)], various representations based on truncated series expansions for the solution interaction parameters [Antypas (31), Brebrick (32), Rao & Tiller (33)], and the quasichemical model [Stringfellow & Greene (34)]. At present, practically all of the available data in III–V systems are restricted to the phase boundaries where composition and temperature both vary simultaneously. As a result, fitting the liquidus line with a given solution model generally does not allow a unique determination of the parameters of the solution model. It is not surprising, therefore, that good agreement with experiment can be claimed for quite different models, especially since deviations from ideality in the III–V systems are relatively small.

An important test for any of the proposed solution models consists of verifying how well they are capable of predicting the vapor pressures over the liquid solutions. At present, reliable pressure measurements along the metal-rich liquidus are available for the Ga-As (35–38), In-As (38), Ga-P (39), and In-P (40, 41)

systems; analyses of these results indicate that the deviations from ideality in these systems are reasonably small over the region where experimental data exist. In addition, it is found (15, 36, 39) that the quantity

$$\alpha = RT \ln \gamma_V/(1-x_V)^2 \qquad 10.$$

where γ_V and x_V are the activity coefficient (determined from vapor pressure measurements) and concentration of the group V element in solution, is a slowly varying function of temperature along the metal-rich liquidus. The simplest model capable of reproducing this observed trend in the activity coefficients is the so-called *simple solution* model, in the terminology introduced by Guggenheim (42). Simple solutions are defined as solutions for which the excess free energy of mixing can be approximated by a parabolic function of composition of the form

$$\Delta G_m^{exc} = \alpha(T,p)x(1-x) \qquad 11.$$

with an interaction parameter α that is a function of temperature and pressure only. This terminology is preferred to *quasiregular solution* because of the usual connotation (43) of the term *regular* with random mixing, without any restriction as to the form of the excess enthalpy functions.

When the liquidus line is calculated using the simple solution model with α as a fitting parameter, it is found again that this parameter must be temperature

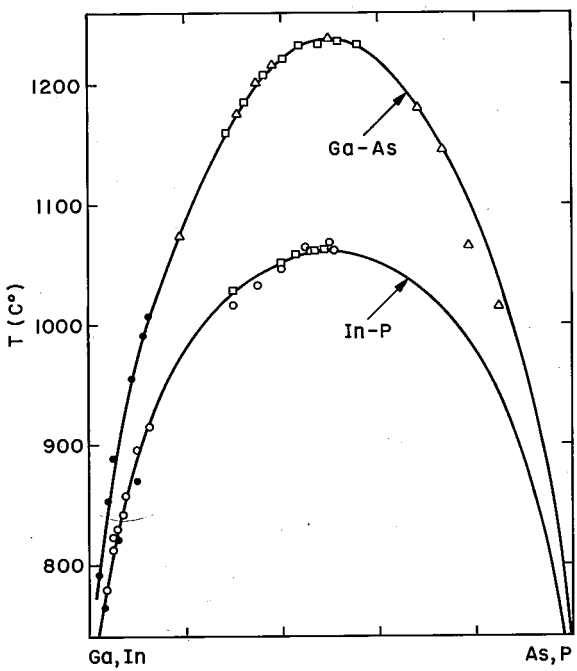

Figure 2 T-x diagram for Ga-As and In-P. After Panish (29). Solid lines from Equation 13.

dependent to obtain a reasonable fit to the experimental data [Thurmond (15)]. This result is illustrated in Figure 3 using the Ga-As and In-P systems as examples. In order for the simple solution model to give a self-consistent description of the phase data, the values of α obtained by fitting liquidus data and those obtained from vapor pressure measurements should be identical, allowing for experimental scatter. Generally, it is found that this is not the case. At present, it is not clear whether this lack of agreement results either from the insufficiency of the model, from the uncertainty associated with some of the thermodynamic constants required in the calculations, or from the fact that an overly simplified liquidus equation that neglects heat capacity contributions is used (39). In particular, Panish (29) observed that a very good agreement between α_V (obtained from vapor pressure data) and α_L (from liquidus data) can be achieved over practically the entire liquidus branch up to the melting point for the Ga-P, Ga-As, and In-P systems by adjusting the reference vapor pressures of pure liquid As and P. Such adjustment does not seem unreasonable, as the experimental determinations for these elements are limited to low temperatures and their extrapolation to higher temperatures may be uncertain because of progressive dissociation in the group V melts.

Although the simple solution model appears to be a useful tool for the interpretation of experimental data in III–V liquids, it should not be inferred that these solutions are in fact simple over their entire concentration range. For some of the lower melting-point compounds the available data suggest that the liquidus is weakly asymmetric around the mid-composition point. If this is indeed the case it is clear that the simple solution representation can apply at best only over certain regions of the phase diagram.

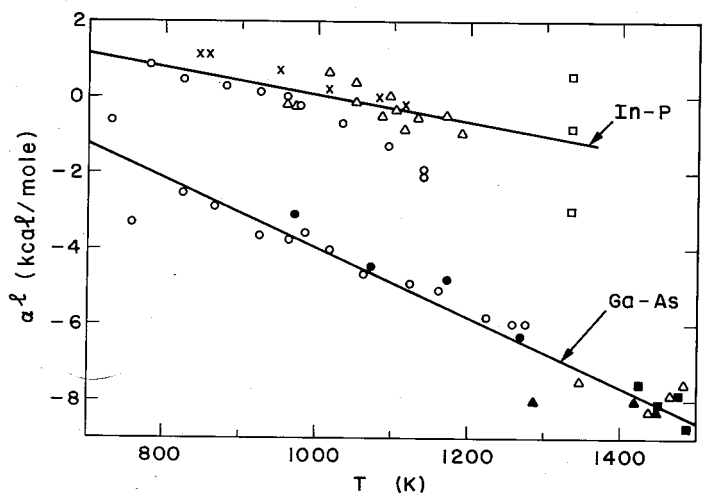

Figure 3 Liquid interaction parameter for Ga-As, In-P versus temperature. α^l calculated at each experimental datum from Equation 13. After Panish (29).

II–VI Liquids

The liquidus curves of the congruently melting II–VI compounds show some similarity with those of the corresponding III–V systems except in the vicinity of the melting point of the compound where the II–VI liquidus exhibits a sharp peak with a small radius of curvature. The Cd-Te and Zn-Te liquidus curves are shown as examples in Figure 4. As a result, if an interaction energy parameter α is calculated along the liquidus curve, it is found that this parameter exhibits a steep minimum near the equiatomic composition instead of the approximately linear or at least smoothly varying temperature dependence found in the III–V systems.

In a study of the liquidus curves of the Zn-Te and Cd-Te systems where this feature is very pronounced, Jordan (46) ascribed this effect to association in the liquid phase, in this case to the presence of the II–VI molecular species, and showed that the steep composition dependence of the interaction energy parameter could be explained in terms of a regular associated solution model. A calculation by Steininger, Strauss & Brebrick (44) of the interaction parameter in the Cd-Te

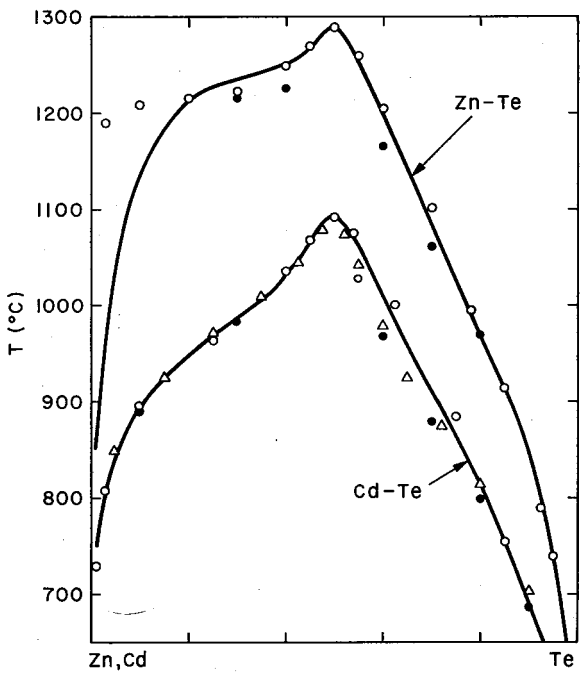

Figure 4 T-x diagram for Zn-Te and Cd-Te. ○ Kulwicki (14), ● Steininger, Strauss & Brebrick (44), △ Lorenz (45). Solid lines from Equation 27. ZnTe: $T^F = 1563$°K, $\Delta S^F = 10.0$ cal/mol°K, $\beta = 0.04$, $\alpha^l = 5.5$ (Zn-branch), 0.2 (Te-branch) kcal/mol; CdTe: $T^F = 1365$°K, $\Delta S^F = 8.8$ cal/mol°K, $\beta = 0.05$, $\alpha^l = -0.011T + 17$ (Cd-branch), 0.5 (Te-branch) kcal/mol.

system using a quasichemical model for the liquid also shows a minimum value for α near the equiatomic composition. The minimum is less steep than that obtained with a regular solution model because the quasichemical representation already incorporates a nonrandom distribution of atom pairs in the liquid, which is weighted according to their interaction energies.

At high temperatures the II–VI compounds sublime into the component gases [Goldfinger & Jeunehomme (47)]. Because of the compound formation in the liquid, the vapor pressures of the elemental components show large (negative) deviations from Raoult's law (expressed in terms of atom fractions) as the congruent melting points are approached. However, when the liquid is treated as a binary mixture A-AB in the A-rich side of the phase diagram, or AB-B in the B-rich side, these deviations are largely eliminated. The concept of a structured liquid phase can therefore account directly for the experimentally determined pressures of the elemental components over the equilibrium liquid [Shiozawa & Jost (48), Jordan & Zupp (49)].

IV–VI Liquids

Four binary IV–VI compounds, SnTe, PbS, PbSe, and PbTe, crystallize in the cubic NaCl structure. A fifth compound, GeTe, is cubic at high temperatures but reverts to the orthorhombic phase upon quenching below ~400°C. The binary T-x phase diagrams for these cubic compounds are similar to those obtained in the high melting point II–VI systems and exhibit a peak in the liquidus curve at the congruently melting compound. Liquidus data (50–52) on the binary Pb-Te and Pb-Se systems are shown as examples in Figure 5. In all cubic systems quoted above, the binary IV–VI molecule is observed as the major vapor species during sublimation of the compound (6, 53).

The similarity between the liquidus curves of the II–VI and IV–VI systems suggests that the latter also possess molecular structure. Recent electromotive force (emf) measurements on liquid Pb-Se solutions by Schneider & Guillaume (54) support this conclusion and show that these liquids behave as mixtures of PbSe with either free Pb or free Se. Calorimetric determinations of partial enthalpies in Sn-Te and Pb-Te liquids (55) also confirm the presence of molecular structures in the liquid.

III–V PHASE DIAGRAMS

Binary Systems

The basic solid-liquid equilibrium condition for a compound AC in equilibrium with a liquid containing A and C is given in terms of the chemical potentials by

$$\mu^s_{AC} = \mu^l_A + \mu^l_C \qquad 12.$$

For III–V liquids with no or negligible association in the liquid phase, a binary liquidus equation was given by Vieland (30), following a more general treatment due to Wagner (56), in the form

$$(\Delta H^F_{AC} - T\Delta S^F_{AC})/RT = -\ln(4x_A x_C) - 2\alpha^l_{A-C}(0.5 - x_A)^2/RT \qquad 13.$$

where ΔH^F is the heat of fusion, ΔS^F the entropy of fusion, and T^F the temperature of fusion of the compound. This liquidus equation was originally derived for the case of a *s*-regular liquid solution; it remains valid (39) for simple solutions with linearly temperature-dependent interaction parameters of the form $\alpha = a + bT$ (linear-simple solutions) but not for other more general solution models (57). In the derivation of Equation 13 the heat capacity difference between the solid phase and a liquid phase of the same composition is neglected and the solid composition is assumed to remain constant. Equation 13 can be rewritten in terms of the liquid activities

$$(\Delta H^F_{AC} - T\Delta S^F_{AC})/RT = -\ln (a^l_A a^l_C / a^{slAC}_A a^{slAC}_C) \qquad 14.$$

where the superscript *sl* indicates that the corresponding activities must be evaluated at the stoichiometric liquid composition $x_A = x_C = 0.5$. The validity of Equation 14 is again restricted to regular or linear-simple solution models. The equation remains valid when extra elements (e.g. dopants, diluents) with negligible solid solubility are present in the liquid, provided the activities a^l_A and a^l_C are calculated accordingly using the expressions for multicomponent systems.

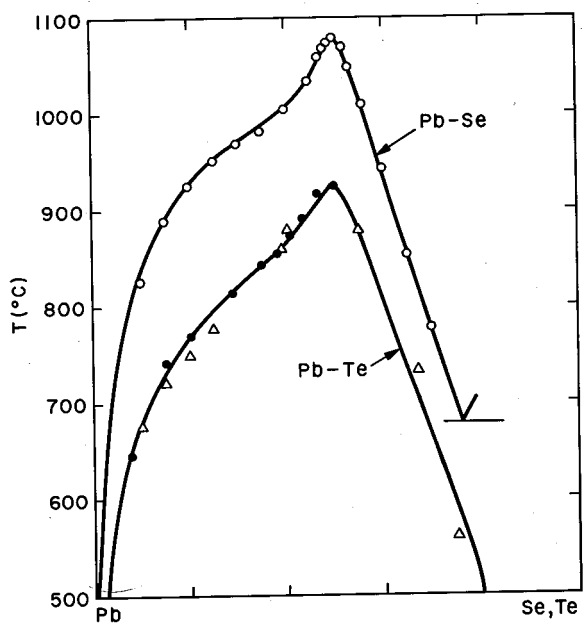

Figure 5 T-x diagram for Pb-Se and Pb-Te. ● Miller & Komarek (50), ○ Seidman (51), △ Lugscheider, Ebel & Langer (52). Solid lines from Equation 27. PbSe: $T^F = 1354$°K, $\Delta S^F = 8.0$ cal/mol°K, $\beta = 0.01$, $\alpha^l = 3.6$ (Pb-branch), -2.25 (Se-branch) kcal/mol. PbTe: $T^F = 1197$°K, $\Delta S^F = 7.85$ cal/mol°K, $\beta = 0.04$, $\alpha^l = 2.6$ (Pb-branch), -2.0 (Te-branch) kcal/mol.

Ternary Systems

In ternary systems where the solid phase of the type $A_xB_{1-x}C$ (or AC_yD_{1-y}) can be treated as a quasibinary solution of the compounds AC and BC (or AC and AD) the basic equilibrium equations are [Ilegems & Pearson (58)]

$$\mu^s_{AC} = \mu^l_A + \mu^l_C; \quad \mu^s_{BC} = \mu^l_B + \mu^l_C \tag{15.}$$

Introducing the activities of the compound components of the solid solution

$$\mu^s_{AC} = \mu^{os}_{AC} + RT \ln a^s_{AC} \tag{16.}$$

and substituting from Equation 14, the equilibrium equations can be rewritten as (58, 59)

$$\begin{aligned} RT \ln (\gamma_{AC} x^s_{AC}) &= RT \ln [x^l_A x^l_C \gamma_A \gamma_C / (\gamma_A^{slAC} \gamma_C^{slAC})] + \Delta S^F_{AC}(T^F_{AC} - T) \\ RT \ln (\gamma_{BC} x^s_{BC}) &= RT \ln [x^l_B x^l_C \gamma_B \gamma_C / (\gamma_B^{slBC} \gamma_C^{slBC})] + \Delta S^F_{BC}(T^F_{BC} - T) \end{aligned} \tag{17.}$$

In these equations all quantities are evaluated at the temperature T and the superscript *sl* refers to the stoichiometric liquid. The activity coefficients γ_i are given, for simple or strictly regular solutions of n components, by (60)

$$RT \ln \gamma_i = \sum_{\substack{j=1 \\ i \neq j}}^{n} \alpha_{ij} x_j - \sum_{j=1}^{n} \sum_{h=j+1}^{n} \alpha_{jh} x_j x_h \tag{18.}$$

where $\alpha_{ij} = \alpha_{ji}$ is the interaction parameter in the binary system *i-j*.

Equation 17 can be solved numerically by computer to give the full liquidus-solidus phase diagram in the primary phase field of the compound alloy, using as input parameters the melting points and entropies of fusion of the end compounds and approximate expressions for the activity coefficients based on fitting the binary data. As previously discussed, a strictly regular representation of the solid solution appears to be adequate to describe the presently available phase data for systems where the heats of mixing are small compared to the enthalpies of formation of

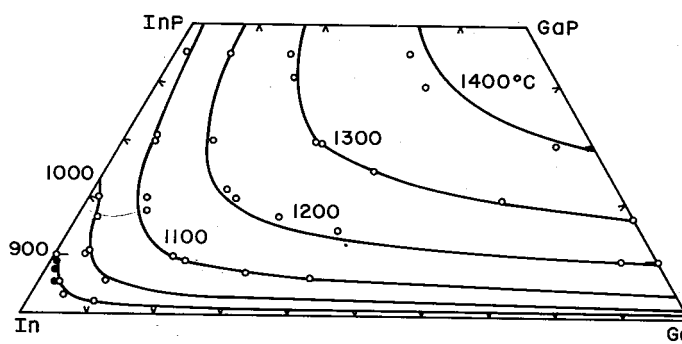

Figure 6 The group III-rich region of the Ga-In-P liquidus. After Panish & Ilegems (1). Solid lines from Equation 17. ○ Panish (64), ● McVittie (28).

the terminal compounds. The interaction parameter α^s in such strictly regular solution representation can be considered as accounting for the effect of second-nearest neighbor interactions between elements on the same sublattice (A and B in the case of $A_xB_{1-x}C$) or, alternatively, for the interactions between binary molecules (AC and BC in $A_xB_{1-x}C$) sharing a common sublattice C. Both these representations are equivalent in the ternary case.

Ternary phase diagram calculations based on Equation 17 have been made for a large number of III–V systems. A summary of this work and of the experimental data available up to mid-1972 has been given by Panish & Ilegems (1). Additional phase diagram information has since then become available on the Al-Ga-P (61), Ga-In-P (62), and Ga-In-Sb (63) systems.

Calculations in (1) were based on a *s*-regular solution representation for the solid and a linear-simple solution model for the liquid. In view of the accuracy of the experimental data and the sometimes important scatter between the experimental data from different overlapping investigations, the use of more complex models does not seem warranted in the ternary case. To illustrate the agreement between experiment and calculations, liquidus and solidus data (28, 64, 65) for one system, Ga-In-P, are shown in Figures 6 to 8 together with calculated results based on Equation 17. The parameters for the calculation are those used in (1). These parameters do not necessarily provide the best possible fit for any given system

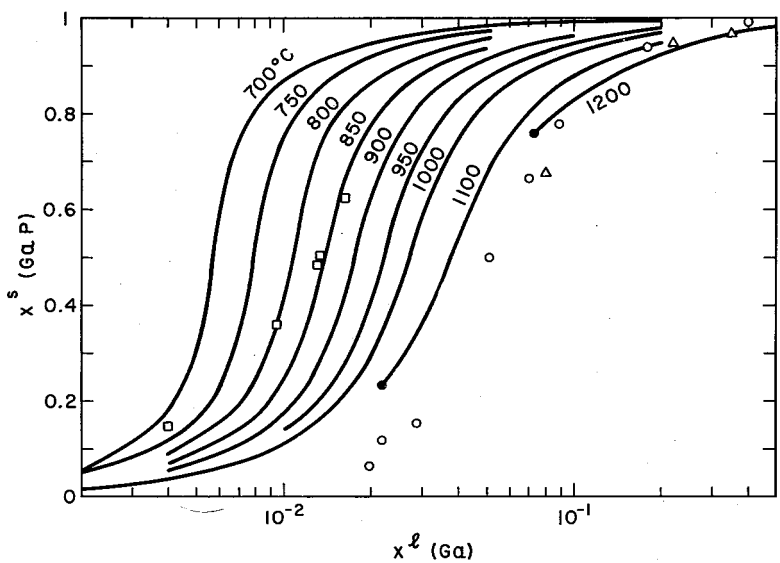

Figure 7 $Ga_xIn_{1-x}P$ solidus as a function of liquidus composition along several isotherms. After Panish & Ilegems (1). ○ 1100–1070°C, △ 1200–1170°C Panish (64), □ 850°C McVittie (28). The slope of the 850°C solidus data is less steep than that predicted by the calculation.

but rather constitute a set of constants that is internally consistent and can be used for the representation of the ensemble of available ternary phase data in III–V systems.

Quaternary Systems with Mixing on Both Sublattices

For quaternary systems of the type $A_xB_{1-x}C_yD_{1-y}$, two solid solution interaction parameters are required in the *s*-regular solution approximation to represent the mixing of A and B on the group III sublattice and of C and D on the group V sublattice. Each parameter can be regarded as representing either interactions between atoms on the same sublattice (e.g. α_1^s representing mixing of A and B) or, equivalently, interactions between ternary compounds (e.g. AC_yD_{1-y} and BC_yD_{1-y} for α_1^s) sharing a common sublattice (e.g. C_yD_{1-y}). At the ternary limits ($y=0$ and $y=1$ for the example given), the values of α_1^s should equal those in the ternary solutions ($A_xB_{1-x}C$ and $A_xB_{1-x}D$ respectively). For intermediate values of y, an interpolation between the terminal values is appropriate; such interpolation is still consistent with the *s*-regular solution model provided the interaction parameters remain independent of the concentrations of the elements being mixed.

With the solid decomposed in its ternary constituents, the equilibrium equations are [Ilegems & Panish (66)]

$$\begin{aligned} &\mu^s(A_xB_{1-x}C) = x\mu_A^l + (1-x)\mu_B^l + \mu_C^l; \quad \mu^s(A_xB_{1-x}D) = x\mu_A^l + (1-x)\mu_B^l + \mu_D^l \\ &\mu^s(AC_yD_{1-y}) = \mu_A^l + y\mu_C^l + (1-y)\mu_D^l; \quad \mu^s(BC_yD_{1-y}) = \mu_B^l + y\mu_C^l + (1-y)\mu_D^l \end{aligned} \qquad 19.$$

An alternate and equivalent set of liquidus equations can be obtained by treating the quaternary solid as a mixture of the binary compounds AC, AD, BC, and BD [Jordan & Ilegems (67)], subject to the restrictions imposed by the crystalline structure of the solid.

Phase diagrams have been experimentally investigated for a number of quaternary alloys with isovalent substitution on both sublattices: AlGaPAs (66), AlGaAsSb [Antypas & Moon (68)], GaInPAs [Antypas & Moon (69)]. Because of the large number of experimental variables, results in these systems will probably remain limited to those areas of the phase diagram that are of practical importance for crystal growth by liquid phase epitaxy.

The advantage obtained in exchange for the increased complexity of composition

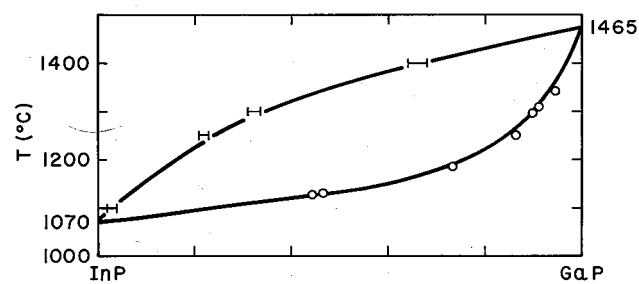

Figure 8 Quasibinary phase diagram for the system GaP-InP. After Panish & Ilegems (1). — Panish (64) ○ Foster & Scardefield (65).

control in these alloys is the ability of growing lattice-matched epitaxial layers on binary substrates over a wide range of alloy composition. In this manner the electronic properties (bandgap, carrier mobility, etc) of the alloy can be controlled over certain ranges while still maintaining good epitaxial growth characteristics. To illustrate this we show in Figure 9 the composition range over which one can expect to grow epitaxial layers of $Ga_xIn_{1-x}P_yAs_{1-y}$ that are lattice-matched to either GaAs or InP, as well as the expected bandgap variation of the alloy over this composition range. The calculation assumes a generalized Vegard law, namely that the lattice constant of the alloy is a linear function of the lattice constants of the binary compounds, weighted according to the number of nearest neighbor bonds (assuming random mixing) of that compound in the crystal. The derived relation is

$$a(A_xB_{1-x}C_yD_{1-y}) = xya_{AC}+x(1-y)a_{AD}+(1-x)ya_{BC}+(1-x)(1-y)a_{BD} \qquad 20.$$

The bandgap variation over the lattice-matched composition range is estimated by averaging the bandgap of the pure constituent compounds and the bowing factors according to the number of nearest neighbor bonds in the crystal in a manner similar to Equation 20

$$E_g = xyE_{AC}+x(1-y)E_{AD}+(1-x)yE_{BC}+(1-x)(1-y)E_{BD} - [c_1x+c_2(1-x)]y(1-y)-[c_3y+c_4(1-y)]x(1-x) \qquad 21.$$

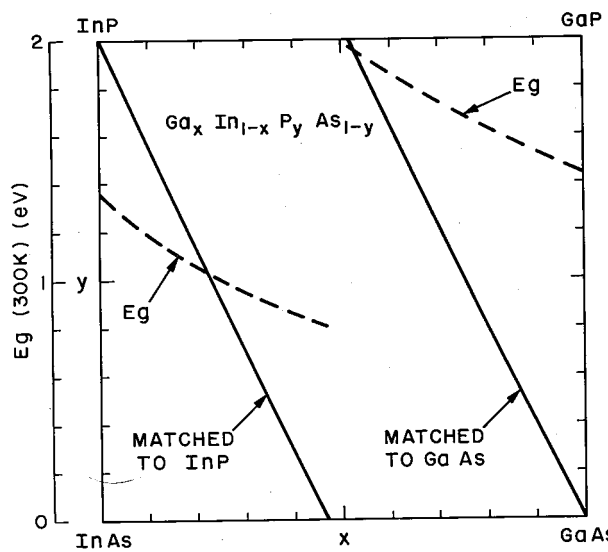

Figure 9 Bandgap (dashed) and composition y (solid lines) versus composition x in the $Ga_xIn_{1-x}P_yAs_{1-y}$ system for quaternary alloys lattice-matched to GaAs on InP substrates (Equation 20, 21). Lattice constants from Giesecke (70). 300°K bandgaps (direct minima) and bowing parameters from Onton (71): E_Γ(eV) = 2.74 (GaP), 1.44 (GaAs), 1.35 (InP), 0.36 (InAs); C(eV) = 0.21 (GaP-As), 0.28 (InP-As), 0.50 (Ga-InP), 0.28 (Ga-InAs).

where c_1, c_2, c_3, c_4 designate the bowing parameters in the ACD, BCD, ABC, ABD systems respectively.

While it is in principle possible to grow lattice-matched alloys over a wide composition range, there generally will be residual strain present in the crystals because of differences between the coefficients of thermal expansion of the alloy and of the substrate. In the case of growth of $Al_{\sim 0.3}Ga_{\sim 0.7}As$ on GaAs, where the lattice match is essentially perfect at a growth temperature of $\sim 800°C$, it has been demonstrated that by slightly mismatching substrate and epitaxial layer at the growth temperature through the addition of P, the amount of strain in the layer at room temperature could be reduced [Rozgonyi, Petroff & Panish (72); Rozgonyi & Panish (73)].

II–VI AND IV–VI PHASE DIAGRAMS

Binary Systems

Assuming the simplest form of association, the liquid phase A-C can be treated as consisting of three components, namely the unassociated A and C atoms and the binary molecule AC. In his study of the Cd-Te and Zn-Te systems, Jordan (46) concluded that the degree of dissociation of the liquid at the melting point was very small. As a first approximation the liquid may therefore be treated as a binary solution of the dimeric AC and monomeric A species in the A-rich part of the T-x diagram up to the melting point and as a solution of AC and monomeric C in the C-rich part.

The basic liquid-solid equilibrium equation is then

$$\mu^{os}_{AC} = \mu^{l}_{AC} \qquad 22.$$

which can be rewritten in terms of the mole fractions and activity coefficients

$$\mu^{os}_{AC} - \mu^{ol}_{AC} = RT \ln \gamma^{l}_{AC} x^{l}_{AC} \qquad 23.$$

Noting that the left hand side of Equation 23 is a function of temperature only, and relating this quantity to its value at the melting point through the entropy of fusion equation, one obtains

$$\mu^{os}_{AC}(T) - \mu^{ol}_{AC}(T) = \mu^{os}_{AC}(T^F) - \mu^{ol}_{AC}(T^F) - (T^F - T)\Delta S^F_{AC} \qquad 24.$$

Finally after substitution the liquidus equation takes the simple form

$$RT \ln \gamma^{l}_{AC} x^{l}_{AC} = RT^F \ln \gamma^{l}_{AC}(T^F) x^{l}_{AC}(T^F) - (T^F - T)\Delta S^F_{AC} \qquad 25.$$

In Equation 25, ΔS^F_{AC} represents the entropy change for the reaction AC(solid) = AC(liquid). This quantity may be approximated by the experimentally measured entropy of fusion in all cases where the liquid solution is strongly associated.

In the hypothesis of complete association $x^{l}_{AC}(T^F) = \gamma^{l}_{AC}(T^F) = 1$ and the liquidus equation reduces to the well-known Schröder-van Laar (74) expression with x^{l}_{AC} given in terms of the external (overall) concentrations of species A and C by $x^{l}_{AC} = x^{l}_{C}/x^{l}_{A}$ in the A-rich part and $x^{l}_{AC} = x^{l}_{A}/x^{l}_{C}$ in the C-rich part of the diagram.

When the association is not complete, one defines a degree of dissociation β, such that at the melting point

$$x^l_{AC}(T^F) = (1-\beta)/(1+\beta) \quad 26.$$

In this case the liquidus equation is rewritten as

$$RT \ln \gamma^l_{AC} x^l_{AC} = RT^F \ln [\gamma^{sl}_{AC}(1-\beta)/(1+\beta)] - (T^F - T)\Delta S^F_{AC} \quad 27.$$

Using an *s*-regular model for the A+AC liquid and assuming complete association, the activity coefficients are given by

$$RT \ln \gamma^l_{AC} = \alpha^l (1 - x^l_{AC})^2 \quad 28.$$

The solution for the liquidus equations thus allows for two fitting parameters: the degree of dissociation at the melting point, β, and a liquid interaction parameter α^l. This latter parameter will in general take on different values in the A-rich and C-rich parts of the diagram. Values of α^l calculated from the available experimental data in the Cd-Te system are plotted against temperature in Figure 10 for $\beta = 0.05$. The data are quite scattered but exhibit a definite temperature trend at least along the metal-rich branch. The value of β was chosen to minimize the peak in α^l values usually observed near the melting point of these systems. Previous best-fit values of β, determined in a somewhat different manner by Jordan (46) for the Cd-Te and Zn-Te systems, ranged from 0.055 to 0.065, showing thereby that these solutions are nearly completely associated. The solid

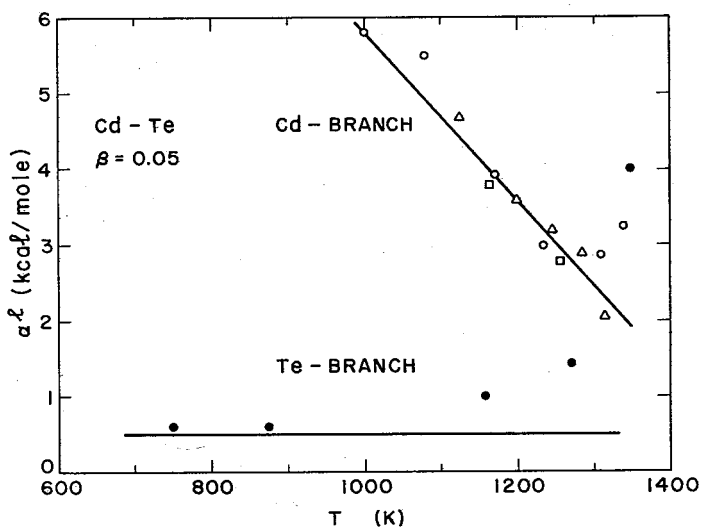

Figure 10 Liquid interaction parameter for Cd-Te versus temperature. α^l calculated at each experimental datum from Equations 27 and 28. ○,● Kulwicki (14), □ Steininger, Strauss & Brebrick (44), △ Lorenz (45).

lines in Figure 4 represent the calculated liquidus based on Equations 27 and 28 using the values of the interaction parameters shown in Figure 10.

A similar calculation of the liquidus interaction parameters along the metal-rich branch is shown in Figure 11 for the Pb-Se and Pb-Te systems. In this case the values of α^l that are obtained appear approximately temperature-independent. Again the dissociation parameter β is adjusted to minimize the increase of α^l near the melting points without, however, completely eliminating the effect. The parameter α^l represents essentially the interaction between AC complexes and the other constituents of the solutions. At low temperatures and along the metal-rich branch, α^l equals $\alpha^l_{AC\text{-}A}$, whereas near the melting point the effects of AC-B interactions need to be included. A constant value of α^l over the entire liquidus branch should therefore not be expected. A good fit to the phase diagram is nevertheless possible using constant values of α^l on each liquidus branch, as shown by the comparison of the calculated curves in Figure 5 with the experimental data.

Ternary Systems

The case where the ternary-associated A, B, C liquid is considered to contain, in addition to the monomeric A, B, and C species, binary-associated molecules of the type AC and BC, can be treated by direct extension of the binary equations given above, as shown by Laugier (23). This treatment neglects the formation

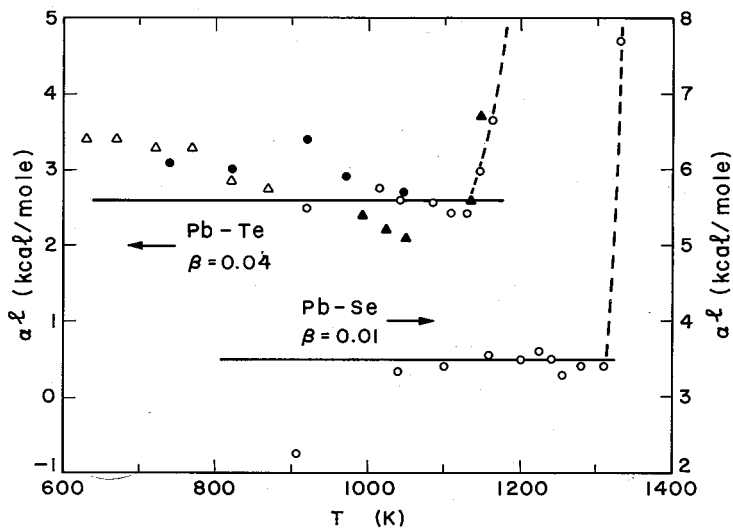

Figure 11 Liquid interaction parameter along metal-rich branch for Pb-Se and Pb-Te versus temperature. α^l calculated at each experimental datum from Equations 27 and 28. Pb-Se: ○ Seidman (51); Pb-Te: ○ Miller & Komarek (50), ● Wagner & Thompson (75), ▲ Lugscheider, Ebel & Langer (52), △ Harris et al (85).

of ternary complexes of the type $A_xB_{1-x}C$ as well as other possible forms of association.

The basic liquid-solid equilibrium equations for this case are

$$\mu^s_{AC} = \mu^l_{AC} = \mu^l_A + \mu^l_C; \quad \mu^s_{BC} = \mu^l_{BC} = \mu^l_B + \mu^l_C \tag{29.}$$

Each of these expressions, developed in a manner analogous to that used to obtain Equation 25, become

$$\begin{aligned} RT \ln a^s_{AC} &= RT \ln \gamma^l_{AC} x^l_{AC} - RT^F_{AC} \ln [\gamma^{sl_{AC}}_{AC}(1-\beta_1)/(1+\beta_1)] + (T^F_{AC} - T)\Delta S^F_{AC} \\ RT \ln a^s_{BC} &= RT \ln \gamma^l_{BC} x^l_{BC} - RT^F_{BC} \ln [\gamma^{sl^{BC}}_{BC}(1-\beta_2)/(1+\beta_2)] + (T^F_{BC} - T)\Delta S^F_{BC} \end{aligned} \tag{30.}$$

where β_1 and β_2 represent the degrees of dissociation at the melting point of the pure compounds AC and BC respectively. Equation 30 defines the liquidus surface in terms of x^l_{AC} and x^l_{BC}. To bring this result to usable form, x^l_{AC}, x^l_{BC} must be related back to the overall (macroscopic) concentrations x^l_A, x^l_B, x^l_C. This is done by considering the second half of the equilibrium Equation 30 in conjunction with a simplified solution model for the quinary liquid. The algebraic treatment is involved and the number of parameters required to describe the 5-component (AC, BC, A, B, C) solution is too large to allow a determination of these parameters by fitting phase data.

A more useful procedure valid for strongly associated liquids consists of considering the limit of complete association ($\beta_1 = \beta_2 = 0$). In this case, for example when $x_A + x_B > x_C$, one considers the liquid as containing only AC, BC, and monomeric A, B, with

$$x^l_{AC} = x^l_A x^l_C/(1-x^l_C)^2; \quad x^l_{BC} = x^l_B x^l_C/(1-x^l_C)^2 \tag{31.}$$

where x_A, x_B, x_C designate, as before, the overall (macroscopic) concentrations of A, B, and C. Having expressed x^l_{AC} and x^l_{BC} in terms of the x_A, x_B, x_C, the remaining problem is that of estimating γ^l_{AC} and γ^l_{BC}. Considering the liquid as a strictly regular or simple quaternary solution, this involves six interaction parameters: $\alpha^l_{AC\text{-}A}$, $\alpha^l_{BC\text{-}B}$, $\alpha^l_{AC\text{-}BC}$, $\alpha^l_{A\text{-}B}$, $\alpha^l_{AC\text{-}B}$, and $\alpha^l_{BC\text{-}A}$. The first four of these can be obtained from analysis of binary and quasibinary data, while the remaining two parameters must be estimated or fitted to ternary results. Once the interaction parameters are determined, the activity coefficients γ_{AC} and γ_{BC} follow directly from Equation 18.

Along the quasibinary ($x^l_C = 0.5$), Equation 30 further simplifies to yield, in the limit of complete association,

$$\begin{aligned} RT \ln x^s_{AC} + \alpha^s(1-x^s_{AC})^2 &= RT \ln (2x^l_A) + \alpha^l(1-2x^l_A)^2 + (T^F_{AC} - T)\Delta S^F_{AC} \\ RT \ln x^s_{BC} + \alpha^s(1-x^s_{BC})^2 &= RT \ln (2x^l_B) + \alpha^l(1-2x^l_B)^2 + (T^F_{AC} - T)\Delta S^F_{AC} \end{aligned} \tag{32.}$$

Equation 32 finally involves only two interaction parameters, α^s and α^l. The equations are formally identical to those that apply in the case of pseudobinary systems without association. This result is expected and underlines again that only limited thermodynamic information can be inferred on the basis of an analysis restricted to the quasibinary sections of the phase diagram.

Pseudobinary liquidus and solidus curves have been determined experimentally for most lower melting point II–VI compound solutions. The phase diagrams for the ZnTe-CdTe, ZnTe-HgTe, CdTe-HgTe, ZnSe-ZnTe, CdSe-CdTe, and HgSe-HgTe systems have been reviewed by Steininger (24) and Laugier (23). The calculation by Laugier assumes an ideal liquid ($\alpha^l = 0$) and uses only α^s as a fitting parameter. These best-fit values have been included in Figure 1. Calculated diagrams for the CdTe-ZnTe and CdTe-CdSe systems based on Equation 32 and using both α^l and α^s as fitting parameters, adjusted to match the calculated curves to the experimental data at mid-composition, are shown as examples in Figure 12. Best-fit values of α^s obtained in this manner are quite different from those of Laugier, demonstrating again that results for α^s depend on the choice of α^l.

In the CdSe-CdTe system, a phase transition from sphalerite to wurtzite occurs at $x(\text{Se}) > 0.2$ (76, 77). In this case each structural region of the diagram should be considered separately. The pseudobinary diagram of Figure 12 neglects the existence of this phase transition as its effect on the overall shape of the characteristic appears to be rather small in this case.

Except for the Zn-Cd-Te system studied by Steininger, Strauss & Brebrick (44), very little or no information exists on ternary II–VI phase diagrams outside the pseudobinary range. Liquidus isotherms in the Zn-Cd-Te system are similar in shape to those found in the corresponding III–III–V systems but show sharp peaks along the pseudobinary ZnTe-CdTe composition line that correspond to the marked increase in temperature near the equiatomic composition.

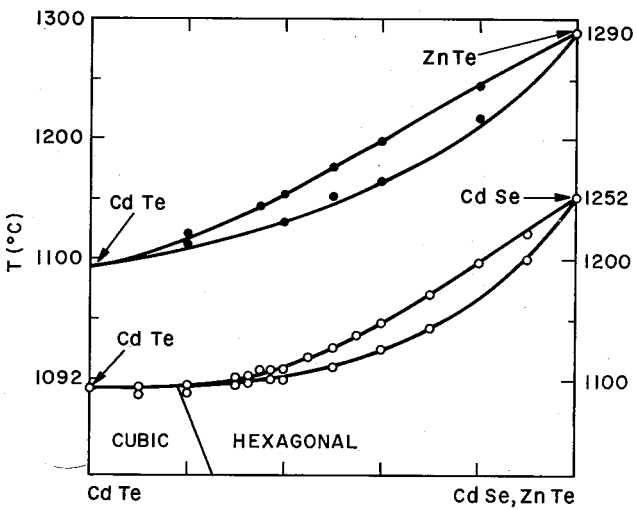

Figure 12 Quasibinary phase diagram for the systems CdTe-ZnTe and CdTe-CdSe. ● Steininger, Strauss & Brebrick (44), ○ Strauss & Steininger (76), Kulwicki (14). Solid lines from Equation 32. Curve fitted interaction parameters (kcal/mol): (Cd, Zn)Te, $\alpha^l = -1.3$, $\alpha^s = 0.1$; Cd(Se, Te), $\alpha^l = -1.25$, $\alpha^s = 0.1$. CdSe: $T^F = 1525°\text{K}$, $\Delta S^F = 6.85$ cal/mol°K. CdTe, ZnTe values as in Figure 4.

Continuous solid solutions are formed between all cubic IV–VI compounds, with the possible exception of the PbS-PbTe system because of the large anion size difference in this case. Liquidus and solidus data have been given for the SnTe-PbTe (78–81), PbS-PbSe (82), and PbSe-PbTe (83) systems. Vegard's law is closely obeyed over the entire composition range. Diagrams for the SnTe-PbTe and PbSe-PbTe systems are shown in Figure 13, together with calculated curves based on Equation 32. As was the case for the II–VI systems, the model allows a reasonable fit to the experimental results, although these liquids are undoubtedly more complex than assumed in the model.

The ternary IV–VI systems Sn-Pb-Se and Sn-Pb-Te have been recently analyzed by Laugier et al (84). For both of these systems a calculated phase diagram was shown to give a reasonable agreement with the then available experimental data along certain cuts of the liquidus surfaces. Recent more complete experimental results in the Sn-Pb-Te system by Harris et al (85) are, however, in serious disagreement with this calculation, especially insofar as the solidus is concerned. These differences may presumably be attributed to the fact that the solution model

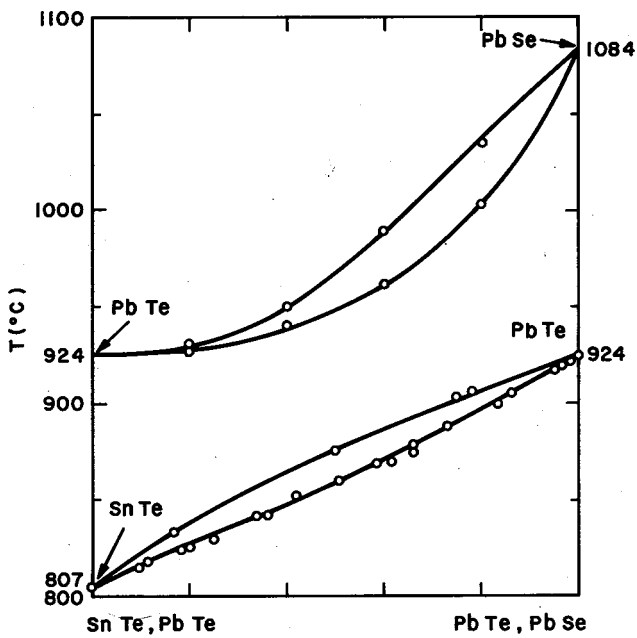

Figure 13 Quasibinary phase diagrams for the systems PbTe-PbSe and SnTe-PbTe. PbSe-PbTe: ○ Steininger (83), SnTe-PbTe: ○ Wagner & Willardson (80), corrected to bring melting points of end compounds in agreement with presently accepted values, ● Calawa et al (79). Solid lines from Equation 32. Curve-fitted interaction parameters (kcal/mol): Pb(Se, Te), $\alpha^l = -1.37$, $\alpha^s = 0.2$; (Sn, Pb)Te, $\alpha^l = 1.55$, $\alpha^s = 1.5$. SnTe: $T^F = 1080°K$, $\Delta S^F = 7.43$ cal/mol°K; PbTe, PbSe values as in Figure 5.

used by Laugier is overly simplified in that the dimeric liquid mixture SnTe-PbTe is treated as ideal and that the ternary interactions SnTe-Pb and PbTe-Sn are neglected. A priori estimates of these different interaction parameters are very uncertain, and it appears therefore that a meaningful phase diagram calculation in these associated systems is not possible without resource to experimental ternary data.

Experimental results (85) and calculated solidus isotherms in the Sn-Pb-Te system are shown in Figure 14. The calculation is based on Equation 30 with, for simplicity, $\beta_1 = \beta_2 = 0$. The interaction parameters $\alpha^s_{\text{SnTe-PbTe}}$, $\alpha^l_{\text{SnTe-PbTe}}$, $\alpha^l_{\text{SnTe-Sn}}$, $\alpha^l_{\text{PbTe-Pb}}$, and $\alpha^l_{\text{Sn-Pb}}$ were obtained respectively from the fits to the pseudobinary (Figure 13) and binary (Figure 5) data and from the measured heats of mixing (86) in the Sn-Pb system. The remaining ternary parameters $\alpha^l_{\text{SnTe-Pb}}$ and $\alpha^l_{\text{PbTe-Sn}}$ were fitted to the experimental data. The agreement is found to be quite good. However, it is likely that other associated species are present in the solution at least in certain regions of the diagram, so that no particular significance should be attached to the values of the ternary parameters.

It is interesting to note that in (85) an excellent fit to the data was obtained with Equation 17 (which applies to ternary systems without association) by empirically adjusting $\alpha^s_{\text{SnTe-PbTe}}$ and $\alpha^l_{\text{Sn-Pb}}$. This result demonstrates again that the comparison

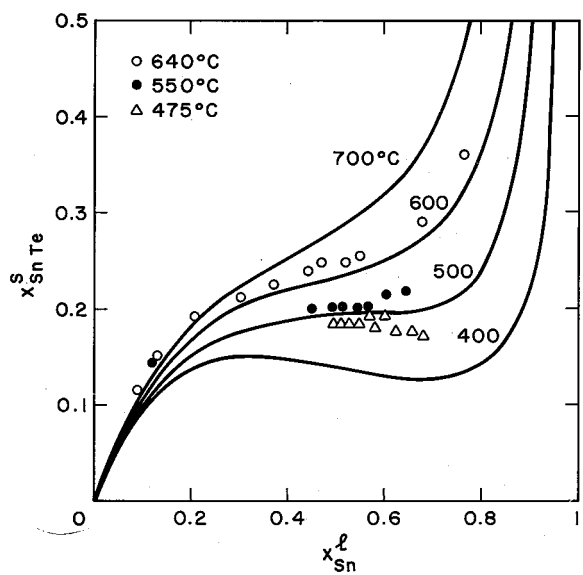

Figure 14 $Sn_xPb_{1-x}Te$ solidus versus liquidus composition along several isotherms. Data from Harris et al (85). Solid lines from Equation 30 with $\beta_1 = \beta_2 = 0$. Interaction parameters (kcal/mol): α^s(SnTe-PbTe) = 1.5, α^l(SnTe-PbTe) = 1.55, α^l(SnTe-Sn) = 3.7, α^l(PbTe-Pb) = 2.6, α^l(Sn-Pb) = 1.32, α^l(SnTe-Pb) = 5.4, α^l(PbTe-Sn) = 7. Other values as in Figures 5 and 13.

between the "fitted" calculated curves and the experimental data does not provide in itself a critical test as to the validity of the model used in the phase diagram calculations, especially when only a limited region of the phase diagram is considered. Nevertheless such calculations are very useful in crystal growth in that they give a reasonable means for interpolation or extrapolation from existing results and provide a unified framework for the analysis of experimental data in compound alloy systems.

CONCLUSION

Because of their unique properties, the compound semiconductor alloys have become firmly established as useful semiconductors whose field of applications is constantly widening. The thermodynamic properties of these systems and their liquid-solid phase diagrams are generally understood. This understanding has aided the development of a growth technology for these alloys to the point where in some of the more useful III–V and IV–VI systems, alloy crystals of quality, comparable to that of the binary compounds, presently can be prepared. A major limitation of the solution growth technique results from the often large differences in the equilibrium compositions of the liquid and solid phases, which lead to gradual compositional variations in the grown crystals. For these reasons continuous growth procedures such as chemical vapor deposition or vacuum evaporation may be expected to play an increasing role in the preparation of thin uniform single crystal alloy films.

Literature Cited

1. Panish, M. B., Ilegems, M. 1972. *Prog. Solid State Chem.* 7:39
2. Stringfellow, G. L. 1975. *MTP Int. Rev. Sci.* To be published
3. Foster, L. M. 1975. *Preparation and Properties of Solid-State Materials*, ed. R. A. Lefever et al. New York: Dekker
4. Kressel, H., Nelson, H. 1973. *Phys. Thin Films* 7:115
5. Mullin, J. B., Hurle, D. T. J. 1973. *J. Lumin.* 7:176
6. Abrikosov, N. K., Bankina, V. F., Poretskaya, L. V., Shelimova, L. E., Skudnova, E. V. 1969. *Semiconducting II–VI, IV–VI and V–VI Compounds*, transl. A. Tybulewicz. New York: Plenum
7. Harman, T. C., Melngailis, I. 1974. *Appl. Solid State Sci.* 4:1
8. Phillips, J. C. 1968. *Phys. Rev. Lett.* 20:550
9. Van Vechten, J. A. 1969. *Phys. Rev.* 182:891
10. Van Vechten, J. A. 1969. *Phys. Rev.* 187:1007
11. Phillips, J. C., Van Vechten, J. A. 1970. *Phys. Rev. B* 2:2147
12. Van Vechten, J. A. 1973. *Phys. Rev. B* 7:1479
13. Lichter, B. D., Sommelet, P. 1969. *Trans. AIME* 245:99, 1021
14. Kulwicki, B. M. 1963. *Phase equilibria of some compound semiconductors by DTA calorimetry.* PhD thesis. Univ. Mich., Ann Arbor
15. Thurmond, C. D. 1965. *J. Phys. Chem. Solids* 26:785
16. Van Vechten, J. A., Bergstresser, T. K. 1970. *Phys. Rev. B* 1:3351
17. Van Vechten, J. A. 1970. *Proc. 10th Int. Conf. on the Physics of Semiconductors*, ed. S. P. Keller, J. C. Hensel, F. Stern, 602. Oak Ridge: US Atomic Energy Comm.
18. Stringfellow, G. B. 1972. *J. Phys. Chem. Solids* 33:665
19. Stringfellow, G. B. 1973. *J. Phys. Chem. Solids* 34:1749
20. Urusov, V. S. 1970. *Inorg. Mater. USSR* 6:1061
21. Brebrick, R. F., Panlener, R. J. 1974. *J. Electrochem. Soc.* 121:932
22. Foster, L. M. 1972. *Electrochem. Soc. Ext. Abstr.* Spring 1972:147

23. Laugier, A. 1973. *Rev. Phys. Appl.* 8: 259
24. Steininger, J. 1970. *J. Appl. Phys.* 41: 2713
25. Foster, L. M., Woods, J. F. 1971. *J. Electrochem. Soc.* 118:1175
26. Foster, L. M., Woods, J. F. 1972. *J. Electrochem. Soc.* 119:504
27. Wu, T. Y., Pearson, G. L. 1972. *J. Phys. Chem. Solids* 33:409
28. McVittie, J. P. 1972. *Liquid epitaxial growth of* $In(1-x)\ Ga(x)P$ *with applications to red light-emitting diodes.* PhD thesis. Stanford Univ., Stanford, Calif.
29. Panish, M. B. 1974. *J. Cryst. Growth* 27:6
30. Vieland, L. J. 1963. *Acta Metall.* 11: 137
31. Antypas, G. A. 1970. *J. Electrochem. Soc.* 117:700
32. Brebrick, R. F. 1971. *Metall. Trans.* 2:1657, 3377
33. Rao, M. V., Tiller, W. A. 1970. *J. Phys. Chem. Solids* 31:191
34. Stringfellow, G. B., Greene, P. E. 1969. *J. Phys. Chem. Solids* 30:1779
35. Richman, D. 1963. *J. Phys. Chem. Solids* 24:1131
36. Arthur, J. R. 1967. *J. Phys. Chem. Solids* 28:2257
37. Foxon, C. T., Harvey, J. A., Joyce, B. A. 1973. *J. Phys. Chem. Solids* 34:1693
38. Pupp, C., Murray, J. J., Pottie, R. F. 1974. *J. Chem. Thermodyn.* 6:123
39. Ilegems, M., Panish, M. B., Arthur, J. R. 1974. *J. Chem. Thermodyn.* 6:157
40. Panish, M. B., Arthur, J. R. 1970. *J. Chem. Thermodyn.* 2:299
41. Bachman, K. J., Buehler, E. 1974. *J. Electrochem. Soc.* 121:835
42. Guggenheim, E. A. 1967. *Thermodynamics,* 197. Amsterdam: North-Holland. 5th ed.
43. Hildebrand, J. H., Prausnitz, J. M. Scott, R. L. 1970. *Regular and Related Solutions.* New York: Van Nostrand
44. Steininger, J., Strauss, A. J., Brebrick, R. F. 1970. *J. Electrochem. Soc.* 117: 1305
45. Lorenz, M. R. 1962. *J. Phys. Chem. Solids* 23:939
46. Jordan, A. S. 1970. *Metall. Trans.* 1: 239
47. Goldfinger, P., Jeunehomme, M. 1963. *Trans. Faraday Soc.* 59:2851
48. Shiozawa, L. R., Jost, J. M. 1971. *Research on Improved II–VI Crystals.* Aerospace Research Laboratories Report ARL 71-0017. Wright-Patterson AFB, Ohio
49. Jordan, A. S., Zupp, R. R. 1969. *J. Electrochem. Soc.* 116:1264, 1285
50. Miller, E., Komarek, K. L. 1966. *Trans. AIME* 236:832
51. Seidman, D. N. 1966. *Trans. AIME* 236:1361
52. Lugscheider, W., Ebel, H., Langer, G. 1965. *Z. Mettalkd.* 56:851
53. Hansen, E. E., Munir, Z. A. 1970. *J. Electrochem. Soc.* 117:121
54. Schneider, M., Guillaume, J. C. 1974. *J. Phys. Chem. Solids* 35:471
55. Castanet, R., Claire, Y., Lafitte, M. 1972. *High Temp. High Pressures* 4:343
56. Wagner, C. 1958. *Acta Metall.* 6:309
57. Jordan, A. S., Weiner, M. E. 1975. *J. Phys. Chem. Solids.* To be published
58. Ilegems, M., Pearson, G. L. 1969. *Proc. 1968 Symp. on GaAs.* London: Inst. Phys.
59. Ilegems, M. 1970. *Liquid epitaxy and physical properties of* $Ga_{1-x}Al_xAs$. PhD thesis. Stanford Univ., Stanford, Calif.
60. Jordan, A. S. 1972. *J. Electrochem. Soc.* 119:123
61. Ilegems, M., Panish, M. B. 1973. *J. Cryst. Growth* 20:77
62. Astles, M. G. 1974. *J. Chem. Thermodyn.* 6:105
63. Antypas, G. A. 1972. *J. Cryst. Growth* 16:181
64. Panish, M. B. 1970. *J. Chem. Thermodyn.* 2:319
65. Foster, L. M., Scardefield, J. E. 1970. *J. Electrochem. Soc.* 117:534
66. Ilegems, M., Panish, M. B. 1974. *J. Phys. Chem. Solids* 35:409
67. Jordan, A. S., Ilegems, M. 1975. *J. Phys. Chem. Solids* 36:329
68. Antypas, G. A., Moon, R. L. 1974. *J. Electrochem. Soc.* 121:416
69. Antypas, G. A., Moon, R. L. 1973. *J. Electrochem. Soc.* 120:1574
70. Giesecke, G. 1966. *Semiconductors and Semimetals,* ed. R. K. Willardson, A. C. Beer, 2:63. New York: Academic
71. Onton, A. 1973. *Festkörper Probleme XIII,* ed. H. J. Queisser, 59. Braunschweig: Vieweg-Pergamon
72. Rozgonyi, G. A., Petroff, P. M., Panish, M. B. 1974. *Appl. Phys. Lett.* 24:251
73. Rozgonyi, G. A., Panish, M. B. 1973. *Appl. Phys. Lett.* 23:533
74. Prigogine, I., Defay, R. 1969. *Chemical Thermodynamics,* 357. London: Longmans. 5th ed.
75. Wagner, J. W., Thompson, A. G. 1970. *J. Electrochem. Soc.* 117:936
76. Strauss, A. J., Steininger, J. 1970. *J. Electrochem. Soc.* 117:1420
77. Vitrikhovskii, N. I., Mizetskaya, I. B., Oleinik, G. S. 1971. *Inorg. Mater. USSR*

7:657
78. Wagner, J. W., Woolley, J. C. 1967. *Mater. Res. Bull.* 2:1055
79. Calawa, A. R., Harman, T. C., Finn, M., Youtz, P. 1968. *Trans. AIME* 242:374
80. Wagner, J. W., Willardson, R. K. 1969. *Trans. Metall. Soc. AIME* 242:366
81. Linden, K. J., Kennedy, C. A. 1969. *J. Appl. Phys.* 40:2595
82. Strauss, A. J., Harman, T. C. 1973. *J. Electron. Mater.* 2:71
83. Steininger, J. 1970. *Metall. Trans.* 1: 2939
84. Laugier, A., Cadoz, J., Faure, M., Moulin, M. 1974. *J. Cryst. Growth* 21:235
85. Harris, J. S., Longo, J. T., Gertner, E. R., Clarke, J. E. 1975. *J. Cryst. Growth.* To be published
86. Hultgren, R., Orr, R. L., Anderson, P. D., Kelley, K. K. 1963. *Selected Values of Thermodynamic Properties of Metals and Alloys.* New York: Wiley